ACES Asian Chemical Editorial Society

doi.org/10.1002/cnma.202300592

CHEMNANOMAT
Research Article

www.chemnanomat.org

# Hexagonal Boron Nitride Spacers for Fluorescence Imaging of Biomolecules

Xiliang Yang,[a] Dong Hoon Shin,[a, d] Ze Yu,[a] Kenji Watanabe,[b] Takashi Taniguchi,[b] Vitaliy Babenko,[c] Stephan Hofmann,[c] and Sabina Caneva*[a]

Fluorescence imaging is an invaluable tool to investigate biomolecular dynamics, mechanics, and interactions in aqueous environments. Two-dimensional materials offer large-area, atomically smooth surfaces for wide-field biomolecule imaging. Despite the success of graphene for on-chip biosensing and biomolecule manipulation, its strong fluorescence-quenching properties pose a challenge for biomolecular investigations that are based on direct optical readouts. Here, we employ few-layer hexagonal boron nitride (hBN) as a precisely tailorable fluorescence spacer between labelled lipid membranes and graphene substrates. By stacking high-quality hBN crystals in the 10–20 nm thickness range on monolayer graphene, we observe distance-dependent fluorescence intensity variations. Remarkably, with hBN spacers as thin as 20 nm, the fluorescence intensity is comparable to bare $SiO_2$/Si substrates, while the intensity was reduced to 60% and 80% with ~10 nm and ~16 nm hBN thicknesses respectively. We confirm that predetermined hBN thicknesses can be employed to control the non-radiative energy transfer properties of graphene, with fluorescence quenching following a $d^{-4}$ distance-dependent behaviour. This seamless integration of electronically active and dielectric van der Waals materials into vertical heterostructures enables multifunctional platforms addressing the manipulation, localization, and visualization of biomolecules for fundamental biophysics and biosensing applications.

## Introduction

Fluorescence imaging has emerged as a key tool that can reveal accurate quantitative and mechanistic insights into biomolecule dynamics, mechanics, and interactions down to the single-molecule level.[1–3] This technique has proven invaluable in providing a detailed understanding of the inner workings of complex biological structures and functions[4] such as ribosomal dynamics and assembly[5] as well as protein folding and binding.[6] Its simple implementation, molecular specificity and compatibility with multicolour, multiplexed imaging has led it to be routinely used in biophysics research.

Monitoring molecular properties, conformations and spatial arrangements can be done either by measuring freely-diffusing molecules or molecules that are spatially constrained. Constraining can include tethering to surfaces and/or beads,[7] and while it enables longer observation times during imaging, it may not fully represent the behaviour of native biomolecules. An ideal scenario is to present biomolecules with a non-strongly interacting surface that provides reversible attachment sites through adsorption, while not interfering with biological function. Such surfaces would offer sufficient binding strength for molecules to be localized and tracked during in-plane imaging, yet allow sufficient mobility, thereby still enabling diffusion, intermolecular interactions and desorption. Two-dimensional (2D) van der Waals (vdW) materials are emerging as promising substrates for biophysical studies. Owing to their atomically-smooth surfaces free of dangling bonds, biocompatibility and transparency in their few-layer form, they represent novel platforms to obtain statistically-relevant datasets of biological properties and interactions over large surface areas.

Within the class of vdW materials, graphene has been extensively studied in the context of biosensor devices. It has been used in various implementations including as an electrode material for the dielectrophoretic trapping of DNA,[8] as a surface sensor in FETs,[9] and as a membrane for nanopore and tunnelling based sensing.[10] The development of graphene for bioimaging is, however, not without challenges. Strong fluorescence quenching of fluorophores by graphene poses a significant obstacle to its use in fluorescence-based optical readouts. While its excellent fluorescence suppression properties have been employed in resonance Raman spectroscopy to weaken the background fluorescence emission and enhance the Raman peaks from biomolecules,[11] and in the generation of quenching masks for deterministic positioning of hBN quantum emitters, they hinder direct fluorescence-based

[a] X. Yang, Dr. D. H. Shin, Dr. Z. Yu, Dr. S. Caneva
Department of Precision and Microsystems Engineering
Delft University of Technology
Mekelweg 2, 2628 CD, Delft, The Netherlands
E-mail: s.caneva@tudelft.nl

[b] Dr. K. Watanabe, Dr. T. Taniguchi
National Institute for Materials Science
1-1 Namiki, Tsukuba, Ibaraki 305-0044 Japan

[c] Dr. V. Babenko, Prof. Dr. S. Hofmann
Department of Engineering
University of Cambridge
Cambridge CB3 0FA, UK

[d] Dr. D. H. Shin
Present address: Department of Electronics and Information Engineering, Korea University, Sejong 30019, Republic of Korea

imaging.[12] For example, the measured emitter decay rate for rhodamine molecules is enhanced 90 times (energy transfer efficiency of ~99%) at distances d ~5 nm with respect to the decay in vacuum.[13] This high energy transfer rate is mainly due to the two-dimensionality and gapless character of the monatomic graphene.[14]

To minimize quenching, it is essential to place an inert spacer material between the fluorophore and the graphene layer. Since fluorescence quenching is highly sensitive to the distance,[13,15] the spacer's thickness needs to be precisely controlled. Nanoscale spacers with tunable graphene-dye separation have been generated with DNA origami nanostructures anchored on graphene monolayers and functionalized with single fluorophores (Atto542, Atto647N). These structures show a strong distance-dependent quenching behaviour proportional to $d^{-4}$.[15–16]

In general, large-area spacer materials should be of high quality, i.e. free of pinholes, to prevent defect-mediated quenching.[17–18] Traditional materials for spacer layers include polymers such as polymethylmethacrylate (PMMA) and ceramics, most notably titanium oxide ($TiO_2$), silicon dioxide ($SiO_2$) and silicon nitride ($Si_3N_4$).[13,19–21] Polymers, however, are challenging to precisely deposit with atomic level control.[22] In contrast, ceramic coatings can be generated with high precision by atomic layer deposition, chemical vapor deposition or electron beam evaporation.[13,19–20] Experimental results, however, have shown that achieving atomic control over the spacer thickness while retaining uniformity over large areas is challenging with these methods. This can result in unwanted defects, such as pinholes or point defects, that provide fluorescence quenching pathways. To circumvent this issue, materials that maintain a high degree of crystallinity when scaled down to their few-atomic layer form are needed to retain the optical signatures from labelled biomolecules. A material that is garnering significant attention as an ultraflat, chemically inert and biocompatible substrate is hexagonal boron nitride (hBN). Due to its wide bandgap in the visible, hBN does not act as an non-radiative acceptor and can thus be used in measurements requiring fluorescence emission. Atomically thin hBN has previously been employed as a spacer to improve the metal-enhanced fluorescence of fluorophores on Ag nanoparticles,[23] indicating the suitability of this material as an atomically smooth substrate for fluorescence imaging of biomolecules. hBN has recently also been used in single-molecule imaging, enabling the tracking of single-stranded DNA over long time periods, which revealed anomalous diffusion along hBN terraces.[24]

Here we experimentally demonstrate the use of high quality hBN layers of controlled nanoscale thickness as spacers to prevent quenching of the fluorescence emission from labelled lipid membrane deposited on graphene substrates. Graphene and hBN are highly commensurate, with the lattice constants differing by ~1.6%[25] facilitating the integration of these materials in vertical heterostructures. Another significant advantage is that no specific attachment chemistry is needed to generate the heterostructure and to position molecules at precise distances from the surfaces, as is typically required for DNA origami/graphene[15] and DNA origami/MXene structures.[26]

We perform our imaging study by deterministically stamping defect-free hBN flakes of various thicknesses on a monolayer CVD graphene domain. Monolayer graphene was chosen in order to keep a consistent fluorescence baseline, given that the energy transfer rate increases significantly with the number of graphene layers.[14] With this approach we achieve atomic-level control of the donor (fluorophore) and acceptor (graphene) distance and reveal a distance-dependent scaling of the fluorescence intensity with hBN thicknesses in the range of 10–20 nm. We measure a significant enhancement in fluorescence intensity compared to direct molecule deposition on graphene, with an increase of 60% and 80% achieved by using hBN spacers with thicknesses of 10 nm and 16 nm, respectively. Notably, when the thickness reaches 20 nm, the fluorescence intensity matches that on $SiO_2$/Si substrates where no quenching is expected. The advantage of this 2D material stacking approach is two-fold: 1) it enables the integration of graphene's remarkable electronic functionality with 2) hBN's fluorescence imaging-compatible properties. Combining these two distinctive materials offers a new platform for bio-optoelectronic nanodevices, which can precisely manipulate, localize, and visualize biomolecules on-chip. Importantly, it can significantly expand analytical biosensor capabilities by providing a pathway to investigate the intricate dynamics of biomolecular interactions at the ultimate resolution i.e. at the single-molecule level.[24]

## Results and Discussion

To image the interaction of fluorescently labelled biomolecules with 2D material surfaces, we use fluorescent lipid membranes that are obtained through the giant unilamellar vesicles (GUVs) splashing method. Figure 1a schematically shows the molecular

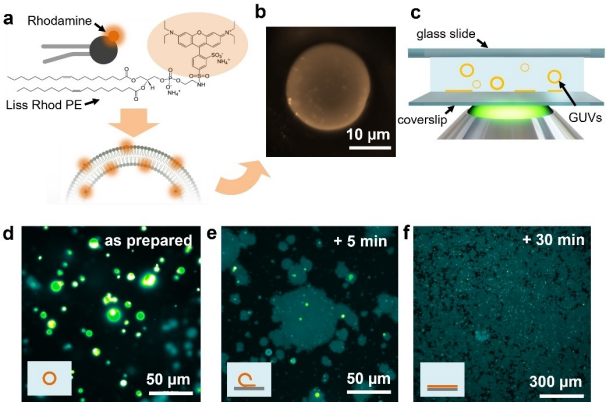


**Figure 1.** (a) Chemical composition and schematic of rhodamine labelled PE lipids (Rh-PE) used in the preparation of fluorescent GUVs. (b) Fluorescence image of a representative GUV obtained with the swelling method. (c) Schematic of the optically accessible flowcell consisting of a liquid chamber between a glass slide and a coverslip. Fluorescence images obtained under 525 nm illumination for (d) as prepared GUVs, (e) GUVs incubated for 5 min and (f) GUVs incubated for 30 min.

composition of rhodamine-labelled phosphatidylethanolamines (PE) lipids and their incorporation into (diphytanoylphosphatidylcholine) DPhPC-based GUVs using the PVA-assisted swelling method.[27] This approach yields large numbers of GUVs with typical diameters of ~20–200 μm. Figure 1b shows an epifluorescence microscopy image of a representative GUV produced with this method recorded under 525 nm illumination. To induce and concurrently image the formation of large area lipid bilayers on glass and $SiO_2$/Si substrates, we prepare a flowcell consisting of a top glass slide separated from a bottom coverslip (150 μm thickness) by parafilm spacers (Figure 1c). The distance between the two glass layers is ~150 μm. Liquids can be introduced into the middle chamber through capillary forces by approaching a pipette tip near the edge of the stack. The flowcell is first filled with a solution of 30 mM NaCl, and GUVs are then flushed into the pre-filled chamber. The flowcell is mounted onto an inverted fluorescence microscope (Nikon Ts2R FL) and images of the bilayer formation process are acquired immediately after insertion and after 5 min and 30 min incubation time. We used a 60× water immersion objective (CFI Pan Apochromat VC) and a 10× (CFI Pan Apochromat Lambda) for imaging. Initially, GUVs freely diffuse in solution (Figure 1d), then they sink to the bottom surface where they rupture due to surface tension effects,[28] and form islands of planar lipid bilayers (Figure 1e). With increasing time, more surface area becomes covered by lipid bilayers, which eventually fuse to form an almost homogeneous film due to lateral diffusion of lipid molecules (Figure 1f). After 30 min, the chamber is flushed with 30 mM NaCl to remove any unruptured freely-diffusing GUVs from the liquid. This ensures that the fluorescence intensity originates only from the deposited film. The same procedure is performed with $SiO_2$/Si substrates with and without graphene. Since the substrates are not transparent, the GUVs are first allowed to rupture on the substrate for 30 min, and then the sample is flipped upside down such that the lipid bilayer can be imaged from below.

Due to their different optical and electronic properties, 2D materials such as graphene and hBN show strikingly different interactions with labelled molecules. We demonstrate the differences by preparing substrates with both materials and subsequently depositing fluorescent lipid membranes on them. The graphene/$SiO_2$/Si substrates are prepared by transferring CVD grown graphene domains (typical diameter of ~200 μm) or monolayer films from the copper foil growth substrate to $SiO_2$/Si chips ($0.7\times0.7$ cm$^2$) using the PMMA-assisted, metal etching method.[29] Figure 2 compares fluorescence images from three different substrates (bare, with graphene domains and with full coverage graphene) before (a, c, e) and after (b, d, f) GUV splashing. As expected, none of the substrates exhibits fluorescence without GUVs in the flowcell. After GUV incubation, the bare Si substrate displays relatively uniform fluorescence. The substrates with graphene, however, display fluorescence only over the areas without graphene coverage, as indicated by the dark hexagonal graphene domains against the bright Si background. Similarly, the full coverage graphene substrate appears dark all over the surface apart from a corner where the graphene film edge is just visible and beyond which

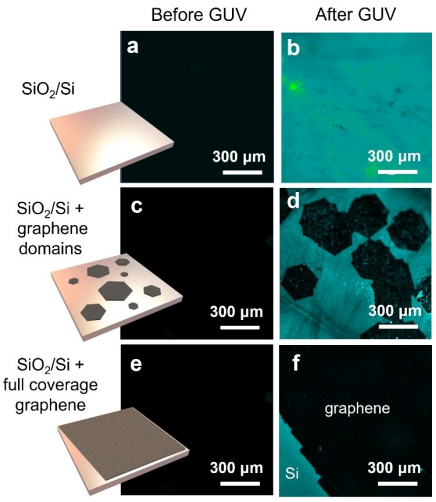


**Figure 2.** (a, c, e) Fluorescence images of bare $SiO_2$/Si, graphene domains on $SiO_2$/Si and full coverage monolayer graphene on $SiO_2$/Si respectively before GUV deposition. (b, d, f) Corresponding images after GUV deposition. The dark areas correspond to the location of the graphene.

the fluorescence intensity is recovered on the $SiO_2$/Si. The absence of fluorescence signal on graphene can be attributed to either the absence of lipid molecules on the domains or the quenching of fluorescence on the carbon layer. Previous studies on lipid deposition on graphene established that various configurations, including inverted lipid bilayers[30] and lipid monolayers,[31–32] rather than bilayers, are formed on graphene due to the effective hydrophobicity of transferred graphene.[33–34] Thus the effects observed in our experiments are attributed to quenching. This is in line with reports demonstrating that in the proximity of fluorescent emitters (e.g. fluorophores, QDs), graphene acts as an efficient energy sink (i.e. fluorescence quencher), efficiently coupling to the emitter via a distant-dependent, non-radiative energy transfer.[12,19–20,35–36]

## hBN as an Atomically Precise Fluorescence Quenching Barrier

In order to establish to what extent the fluorescence quenching of the lipid molecules adsorbed on the graphene can be blocked with a physical distance, we introduce hBN as a spacer layer of precise thickness to separate the rhodamine-labelled lipids from the graphene. hBN is chosen as a spacer given its two-dimensional structure which is highly compatible with stacking onto graphene, thickness control at the atomic level, defect-free quality with surfaces devoid of dangling bonds, high affinities to aromatic fluorophores via $\pi-\pi$ interactions, good chemical stability, and excellent impermeability.

We first transfer a large monolayer graphene domain on $SiO_2$/Si and then use the viscoelastic stamping method[37] to deposit exfoliated hBN flakes (high-temperature high-pressure crystals, NIMS, Japan) onto the edges of the graphene. This allows the subsequent comparison of areas where hBN is in direct contact with the Si and areas where there is a graphene underlayer. Figure 3a shows an optical image of the sample

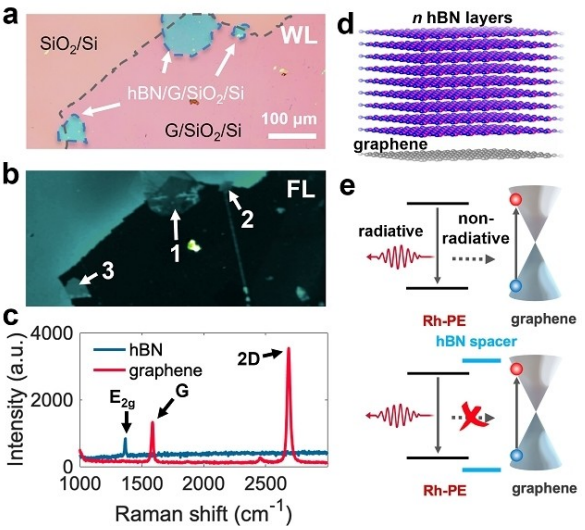


**Figure 3.** (a) White light (WL) optical image of three hBN flakes (blue) stamped on the edge of a large monolayer graphene domain (dark pink). (b) Fluorescence (FL) image of the same areas in (a) measured under 525 nm illumination. (c) Raman spectra of hBN and graphene displaying the characteristic hBN $E_{2g}$ peak and the graphene G and 2D peaks. (d) Structure and arrangement of the vertical hBN/graphene (hBN/G) stacks. (e) Schematic electronic band structures of rhodamine, hBN and graphene, showing the principle of hBN as a fluorescence quenching barrier.

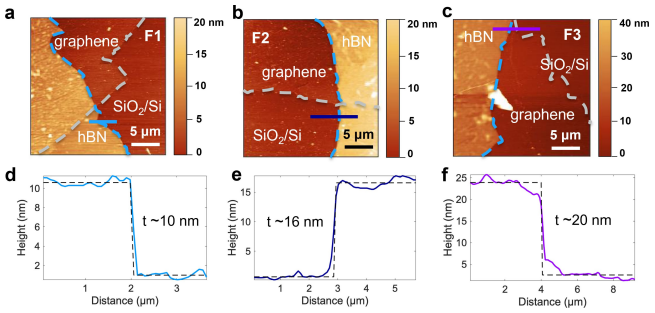


**Figure 4.** AFM imaging of hBN/graphene stacks on $SiO_2$/Si. Tapping mode AFM topography images of (a) Flake 1, (b) Flake 2 and (c) Flake 3. (d–f) hBN height profiles measured at the position of the coloured lines in the corresponding images, with the fitted heights displayed in the graphs.

with three hBN flakes (blue) on graphene (dark pink, right hand side). The corresponding image viewed under 525 nm illumination is shown in Figure 3b. Here, we note that the hBN flakes regions that are on the Si have fluorescence levels similar to that of the bare Si, while the regions on the graphene have lower intensity, however, they are not fully quenched as is the case on the graphene with no hBN. Figure 3c plots the Raman spectra of the graphene and hBN displaying the characteristic G and 2D peaks for monolayer graphene and the $E_{2g}$ peak for hBN, attesting to the high quality of the material after transfer and before GUV deposition. The material dependent fluorescence emission and quenching effects of the hBN/G stacks (Figure 3d) can be understood in the context of the electronic band structures, schematically shown in Figure 3e. Given its gapless band structure, graphene acts as a non-radiating acceptor that directly quenches the donor (rhodamine) emission. Conversely, hBN is a wide (~6 eV) bandgap material which does not emit in the visible and to which the fluorescence energy from the rhodamine cannot be transferred.[38] hBN layers can therefore serve as barriers that inhibit non-radiative energy transfer from the excited rhodamine molecule to graphene.

We perform atomic force microscopy (AFM) imaging to determine the hBN flake thicknesses and to subsequently establish the fluorescence intensity of the hBN/graphene regions as a function of hBN thickness. Figure 4a,b,c show tapping mode topography images of the three flakes (F1, F2, F3) and the corresponding height profiles (Figure 4d, e, f) taken at the position of the coloured lines, from which we extract hBN flake thicknesses (t) of ~10, ~16 and ~20 nm.

After lipid deposition, we quantify the fluorescence intensity levels by taking the average intensity from regions with graphene/$SiO_2$/Si, hBN/graphene/$SiO_2$/Si, and bare $SiO_2$/Si (Figure 5a,b). The normalized intensity histograms from the selected areas range from I = 0 i.e. complete quenching on graphene, to I = 1 i.e. maximum fluorescence that can be

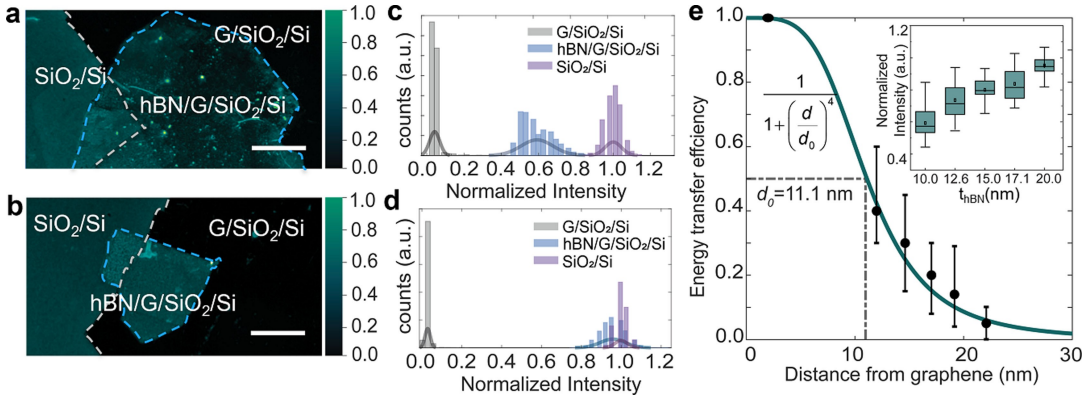


**Figure 5.** Tunable fluorescence intensities on hBN/graphene stacks. (a,b) Fluorescence (FL) images of Flake 1 and Flake 3 under 525 nm illumination after GUV deposition. Scar bar: 30 μm. (c,d) Histograms of the average fluorescence intensity from G/$SiO_2$/Si, hBN/G/$SiO_2$/Si, and bare $SiO_2$/Si regions for Flake 1 and Flake 3 respectively. (e) Normalized energy transfer efficiency as a function of the distance of the fluorophores from the graphene, insert figure: Normalized average fluorescence intensity of hBN/G/$SiO_2$/Si as a function of hBN flake thickness.

achieved on $SiO_2$/Si (Figure 5c,d). On the regions with hBN spacer layers, we observe a fluorescence intensity that is dependent on the thickness of the hBN flakes. To quantify this effect, Figure 5e plots the energy transfer efficiency calculated from hBN/G/$SiO_2$/Si intensity as a function of distance from graphene to excited rhodamine molecule for the three flakes. It is crucial to note that the energy transfer distance encompasses not only the thickness of hBN but also factors in the thickness of a monolayer lipid membrane (~2 nm)[39] since lipid monolayers or inverted lipid bilayers are typically formed on 2D materials due to their largely hydrophobic properties.[32–33] Strikingly, for hBN spacers down to 20 nm, the fluorescence exhibits an intensity level that is comparable to that of lipids directly deposited on $SiO_2$/Si substrates. hBN spacers of ~16 nm display 80% of the $SiO_2$/Si fluorescence level, while this value drops to 60% for hBN thicknesses of ~10 nm. We note that the bright spots on the hBN are usually attributed to polymer residues that are transferred during stamping, which also appear bright under 525 nm illumination wavelength.[40–41]

These results are in good agreement with previous theoretical[13] and experimental[15] studies on Förster-like resonance energy transfer from an excited state of a donor dye molecule to a graphene acceptor substrate. The energy transfer rate depends on the dimensionality of the donor and the acceptor material. For (i) two single-point dipoles, (ii) one line of dipoles and one single-point dipole and (iii) a 2D dipole array, the transfer efficiencies are functions of $d^{-6}$, $d^{-5}$ and $d^{-4}$ respectively. As expected, our experimental data follows a $d^{-4}$ distance-dependent behaviour with a 50% energy transfer efficiency at a distance ($d_0$) of 11.1 nm.

## Conclusions

While graphene has been successfully integrated as an electronic component for biosensing and biomolecule manipulation, for instance in field effect transistors (FETs),[9,42] plasmonic biosensors,[43] nanopores[44] and dielectrophoretic (DEP) trapping devices,[8,10] fluorescence-based sensors have lagged behind, hindered by the quenching properties of the zero-bandgap material. In this work we demonstrate a simple and scalable approach to circumvent this limitation. We identify hBN as a tunable spacer layer that can be stacked on graphene to prevent quenching of fluorescently labelled biomolecules. This occurs due to blocking of the non-radiative energy transfer pathway that otherwise takes place between the excited fluorophore and graphene. A key aspect of this approach is the ability to customize the thickness of the hBN spacer with atomic thickness control, which plays a key role defining the degree of fluorescence intensity that is measured. By depositing fluorescent lipid membranes on the hBN/graphene stacks we demonstrate that an hBN spacer thickness down to 20 nm enables fluorescence emission intensity on a level comparable to that on $SiO_2$/Si substrates without graphene. Spacers with thicknesses of ~16 nm and ~10 nm achieve up to 80% and 60% of the maximum signal.

This work provides valuable insights into optimizing hBN spacer thickness for different biomolecular imaging applications. We foresee particular interest for the single-molecule biophysics field, where studying the inter- and intra-molecule dynamics and mechanics at individual molecule level could be done directly on-chip in a high throughput manner using wide-field fluorescence imaging. By preventing fluorescence quenching, hBN spacers not only enable optical detection and tracking of biomolecules in space and time in physiological conditions but are also compatible with concurrent biomolecule manipulation techniques based on other 2D materials e.g. dielectrophoretic trapping devices with graphene electrodes.[8]

In summary, the utilization of hBN spacer layers for fluorescence imaging of biomolecules is a low-cost, low-complexity approach to achieve biomolecule imaging on electronic materials that are otherwise efficient fluorescent quenchers. The capability to tailor hBN spacer thickness enables the tuning of the fluorescent signal intensity and can be used as a vertical nanoscale ruler in single-molecule studies. Furthermore, the ease of integration with other 2D materials makes this approach versatile and compatible with orthogonal characterization and manipulation techniques, opening exciting new prospects in basic and applied biophysics and nanofluidics research.

## Experimental methods

Lipid layer preparation: The swelling method is carried out in the following steps. First, glass coverslips are coated with a film of 5% PVA (Polyvinyl alcohol) and baked at 60 °C for one hour. Afterwards, a solution of fluorescent lipids is pipetted and spread over the slides. This lipid solution is made by adding 1 μL of 0.1 mg/mL fluorescently labelled lipids (Egg Liss Rhod PE, Avanti Polar Lipids) to 25 μL of 5 mg/mL non-labelled diphytanoyl DPhPC lipids dissolved in chloroform. The fluorescent phosphatidylethanolamines PE lipids are chemically modified with rhodamine dye molecules. For each batch of GUVs, 10 μL of fluorescent lipids solution is used to cover the PVA-coated slides. The slides are left in the desiccator at vacuum for 40 minutes to dehydrate the samples. Subsequently, 200 μL of sucrose (300 mM) is pipetted on the covered slides on which the GUVs are allowed to swell in a petri dish covered by the aluminium foil for one hour. Finally, the GUVs in sucrose are gently collected with a pipette and stored in an epi tube for subsequent imaging.

## *Acknowledgements*

D.H.S. and S.C. acknowledge funding from the European Union's Horizon 2020 research and innovation program (ERC StG, SIMPHONICS, Project No. 101041486). S.C. acknowledges a Delft Technology Fellowship. X.Y. acknowledges funding from the Chinese Scholarship Council (Scholarship No. 202108270002). Z.Y. acknowledges funding from NWO (Project MechanoPore).

## *Conflict of Interests*

The authors declare no conflict of interest.

## Data Availability Statement

The data that support the findings of this study are openly available at https://data.4tu.nl/.

**Keywords:** hexagonal boron nitride (hBN) · graphene · fluorescence · quenching · lipids

[1] S. Weiss, *Science* **1999**, *283*, 1676–1683.
[2] H. Yokota, *Biochim. Biophys. Acta Gen. Subj.* **2020**, *1864*, 129362.
[3] C. Joo, H. Balci, Y. Ishitsuka, C. Buranachai, T. Ha, *Annu. Rev. Biochem.* **2008**, *77*, 51–76.
[4] M. F. Juette, D. S. Terry, M. R. Wasserman, Z. Zhou, R. B. Altman, Q. Zheng, S. C. Blanchard, *Curr. Opin. Chem. Biol.* **2014**, *20*, 103–111.
[5] J. B. Munro, R. B. Altman, C.-S. Tung, J. H. D. Cate, K. Y. Sanbonmatsu, S. C. Blanchard, *Proc. Natl. Acad. Sci. USA* **2010**, *107*, 709–714.
[6] Y. Gambin, A. A. Deniz, *Mol. BioSyst.* **2010**, *6*, 1540–1547.
[7] M. L. Visnapuu, D. Duzdevich, E. C. Greene, *Mol. BioSyst.* **2008**, *4*, 394–403.
[8] A. Barik, Y. Zhang, R. Grassi, B. P. Nadappuram, J. B. Edel, T. Low, S. J. Koester, S. H. Oh, *Nat. Commun.* **2017**, *8*, 1867.
[9] G. Seo, G. Lee, M. J. Kim, S. H. Baek, M. Choi, K. B. Ku, C. S. Lee, S. Jun, D. Park, H. G. Kim, S. J. Kim, J. O. Lee, B. T. Kim, E. C. Park, S. I. Kim, *ACS Nano* **2020**, *14*, 5135–5142.
[10] S. J. Heerema, C. Dekker, *Nat. Nanotechnol.* **2016**, *11*, 127–136.
[11] L. Xie, X. Ling, Y. Fang, J. Zhang, Z. Liu, *J. Am. Chem. Soc.* **2009**, *131*, 9890–9891.
[12] A. Kasry, A. A. Ardakani, G. S. Tulevski, B. Menges, M. Copel, L. Vyklicky, *J. Phys. Chem. C* **2012**, *116*, 2858–2862.
[13] L. Gaudreau, K. J. Tielrooij, G. E. Prawiroatmodjo, J. Osmond, F. J. Garcia de Abajo, F. H. Koppens, *Nano Lett.* **2013**, *13*, 2030–2035.
[14] Z. Chen, S. Berciaud, C. Nuckolls, T. F. Heinz, L. E. Brus, *ACS Nano* **2010**, *4*, 2964–2968.
[15] I. Kaminska, J. Bohlen, S. Rocchetti, F. Selbach, G. P. Acuna, P. Tinnefeld, *Nano Lett.* **2019**, *19*, 4257–4262.
[16] S. Krause, E. Ploetz, J. Bohlen, P. Schuler, R. Yaadav, F. Selbach, F. Steiner, I. Kaminska, P. Tinnefeld, *ACS Nano* **2021**, *15*, 6430–6438.
[17] X. Qin, L. Shen, L. Liang, S. Han, Z. Yi, X. Liu, *J. Phys. Chem. C* **2019**, *123*, 11151–11161.
[18] R. Mrad, M. Poggi, R. Ben Chaabane, M. Negrerie, *J. Colloid Interface Sci.* **2020**, *571*, 368–377.
[19] A. Ghosh, A. Sharma, A. I. Chizhik, S. Isbaner, D. Ruhlandt, R. Tsukanov, I. Gregor, N. Karedla, J. Enderlein, *Nat. Photonics* **2019**, *13*, 860–865.
[20] O. Salihoglu, N. Kakenov, O. Balci, S. Balci, C. Kocabas, *Sci. Rep.* **2016**, *6*, 33911.
[21] K. X. Xie, L. T. Xu, Y. Y. Zhai, Z. C. Wang, M. Chen, X. H. Pan, S. H. Cao, Y. Q. Li, *Talanta* **2019**, *195*, 752–756.
[22] T. Murakami, Y. Arima, M. Toda, H. Takiguchi, H. Iwata, *Anal. Biochem.* **2012**, *421*, 632–639.
[23] W. Gan, C. Tserkezis, Q. Cai, A. Falin, S. Mateti, M. Nguyen, I. Aharonovich, K. Watanabe, T. Taniguchi, F. Huang, L. Song, L. Kong, Y. Chen, L. H. Li, *ACS Nano* **2019**, *13*, 12184–12191.
[24] D. H. Shin, S. H. Kim, K. Coshic, K. Watanabe, T. Taniguchi, G. Verbiest, S. Caneva, A. Aksimentiev, P. G. Steeneken, C. Joo, *bioRxiv* **2023**, *2023.2011*, 2001.565159.
[25] L. H. Li, Y. Chen, *Adv. Funct. Mater.* **2016**, *26*, 2594–2608.
[26] L. Richter, A. M. Szalai, C. L. Manzanares-Palenzuela, I. Kaminska, P. Tinnefeld, *Adv. Mater.* **2023**, *35*, e2303152.
[27] A. Weinberger, F. C. Tsai, G. H. Koenderink, T. F. Schmidt, R. Itri, W. Meier, T. Schmatko, A. Schroder, C. Marques, *Biophys. J.* **2013**, *105*, 154–164.
[28] V. N. Ngassam, W. C. Su, D. L. Gettel, Y. Deng, Z. Yang, N. Wang-Tomic, V. P. Sharma, S. Purushothaman, A. N. Parikh, *Biophys. J.* **2021**, *120*, 586–597.
[29] S. Hofmann, P. Braeuninger-Weimer, R. S. Weatherup, *J. Phys. Chem. Lett.* **2015**, *6*, 2714–2721.
[30] M. Hirtz, A. Oikonomou, T. Georgiou, H. Fuchs, A. Vijayaraghavan, *Nat. Commun.* **2013**, *4*, 2591.
[31] S. R. Tabaei, W. B. Ng, S. J. Cho, N. J. Cho, *ACS Appl. Mater. Interfaces* **2016**, *8*, 11875–11880.
[32] L. M. Lima, W. Fu, L. Jiang, A. Kros, G. F. Schneider, *Nanoscale* **2016**, *8*, 18646–18653.
[33] B. M. Blaschke, P. Bohm, S. Drieschner, B. Nickel, J. A. Garrido, *Langmuir* **2018**, *34*, 4224–4233.
[34] J. Zhang, K. Jia, Y. Huang, Y. Wang, N. Liu, Y. Chen, X. Liu, X. Liu, Y. Zhu, L. Zheng, H. Chen, F. Liang, M. Zhang, X. Duan, H. Wang, L. Lin, H. Peng, Z. Liu, *Nano Lett.* **2021**, *21*, 9587–9593.
[35] M. Lorenzoni, F. Brandi, S. Dante, A. Giugni, B. Torre, *Sci. Rep.* **2013**, *3*, 1954.
[36] J. Kim, L. J. Cote, F. Kim, J. Huang, *J. Am. Chem. Soc.* **2010**, *132*, 260–267.
[37] A. Castellanos-Gomez, M. Buscema, R. Molenaar, V. Singh, L. Janssen, H. S. J. van der Zant, G. A. Steele, *2D Mater.* **2014**, *1*, 011002.
[38] S. Castelletto, F. A. Inam, S. I. Sato, A. Boretti, *Beilstein J. Nanotechnol.* **2020**, *11*, 740–769.
[39] T. Chen, A. Ghosh, J. Enderlein, *Nano Lett.* **2023**, *23*, 2421–2426.
[40] D. G. Purdie, N. M. Pugno, T. Taniguchi, K. Watanabe, A. C. Ferrari, A. Lombardo, *Nat. Commun.* **2018**, *9*, 5387.
[41] M. R. Rosenberger, H. J. Chuang, K. M. McCreary, A. T. Hanbicki, S. V. Sivaram, B. T. Jonker, *ACS Appl. Mater. Interfaces* **2018**, *10*, 10379–10387.
[42] M. T. Hwang, M. Heiranian, Y. Kim, S. You, J. Leem, A. Taqieddin, V. Faramarzi, Y. Jing, I. Park, A. M. van der Zande, S. Nam, N. R. Aluru, R. Bashir, *Nat. Commun.* **2020**, *11*, 1543.
[43] D. Rodrigo, O. Limaj, D. Janner, D. Etezadi, J. García de Abajo, V. Pruneri, H. Altug, *Science* **2015**, *349*, 165–168.
[44] S. J. Heerema, L. Vicarelli, S. Pud, R. N. Schouten, H. W. Zandbergen, C. Dekker, *ACS Nano* **2018**, *12*, 2623–2633.

Manuscript received: December 1, 2023
Revised manuscript received: February 17, 2024
Accepted manuscript online: February 19, 2024
Version of record online: March 8, 2024